Macromolecular Research, Vol. 14, No. 6, pp 588-595 (2006)

The Morphology, Structure and Melting Behaviour of Cold Crystallized Isotactic Polystyrene

Carla Marega, Valerio Causin*, and Antonio Marigo

Dipartimento di Scienze Chimiche, Università di Padova, via Marzolo 1, 35131 Padova, Italy

Received April 27, 2006; Revised September 27, 2006

Abstract: The morphology, structure and melting behaviour of cold-crystallized isotactic polystyrene (iPS) were studied by differential scanning calorimetry (DSC), wide angle X-ray diffraction (WAXD) and small angle X-ray scattering (SAXS). The polymer was found to crystallize according to the dual-lamellar stack model. The two populations of lamellae, along with a melting-recrystallization phenomenon, determined the appearance of multiple melting peaks in DSC traces. The annealing peak was attributed to the relaxation of a rigid amorphous phase, rather than to the melting of crystalline material.

Keywords: isotactic polystyrene, crystallization behaviour, small angle X-ray scattering, wide angle X-ray diffraction, differential scanning calorimetry, multiple endotherms.

Introduction

The multiple melting behaviour of isotactic polystyrene (iPS) has been a matter of study for many researchers since this polymer was first synthesized by Natta and co-workers.

The appearance of a double melting peak was first observed by Boon and co-workers, who explained it as a consequence of the melting-recrystallization phenomenon.[1] Pelzbauer and Manley later reported the appearance of a third melting peak located about 10 °C above the crystallization or annealing temperature. They attributed it to the melting of sterically inhomogeneous species.[2]

A number of hypotheses have been put forth to explain the multiple melting behaviour of semicrystalline polymers. According to the melting-recrystallization model, the lower endotherm is due to the melting of lamellae initially formed in the crystallization, while the higher temperature one is originated by the thick and more perfect lamellae formed by recrystallization of partially melted material.[2-8] Another model links double endotherms to the existence of two populations of lamellae having different distributions of thicknesses.[9-16] The two populations of lamellae can exist in different stacks (dual lamellar stack model)[12,16] or within the same one (lamellar insertion model).[13-15] Different morphologies,[17] different perfection of the crystals[18] or a reorganization in the solid state[19] have also been proposed as explanations to the multiple melting behaviour. Liu and co-workers[20-22] and Xu and co-workers[23] ascribed it to the melting of regions of different stability within the same iPS lamella. The relaxation of a "pseudo-crystalline" or rigid amorphous phase[20-24] has been recently advocated as the origin of the annealing peak.

The present paper is intended as a contribution to the elucidation of the morphology of cold crystallized iPS and of the reasons of its multiple melting behaviour.

Differential scanning calorimetry (DSC) was used to determine the position of multiple endotherms. Wide angle X-ray diffraction (WAXD) and small angle X-ray scattering (SAXS) were employed to determine the structure and morphology of the samples.

Experimental

Samples and Sample Preparation. iPS ($\overline{M}_w$=400,000) was purchased from Sigma Aldrich. The dependence of the crystallization behaviour on crystallization temperature and on time were studied.

Samples were prepared by melting the iPS powder for 5 min at 250 °C in a heating press Mod.TM40M40 (Carrea S.r.l., Genoa, Italy) and subsequently quenching in water and ice, obtaining totally amorphous samples (iPSQ).

iPSQ plaques were then posed in an oven Mod. 2100 High Performance (F.lli Galli G&P, Fizzonasco di Pieve Emanuele, Italy) under N_2 atmosphere, preset at the desired crystallization temperature. Samples were prepared at 150, 160, 170, 180, 190, and 200 °C and were designated as iPS150, iPS160, iPS170, iPS180, iPS190, and iPS200, respectively.

The optimal crystallization time was determined by pre-

*Corresponding Author. E-mail: valerio.causin@unipd.it

liminary DSC measurements.

Time dependent experiments were performed by cold crystallizing iPSQ at 160 °C for 10, 20, 30, 40, 50, and 60 min. These samples were denominated as iPS10t, iPS20t, etc., with the number indicating the duration in minutes allowed for the cold crystallization process.

Differential Scanning Calorimetry (DSC). All the measurements were carried out with a TA Instruments mod. 2920 calorimeter operating under nitrogen atmosphere. Polymer samples weighing about 6 mg closed in aluminium pans were heated up to 250 °C at 10 °C/min.

Indium of high purity was used for calibrating the DSC temperature and enthalpy scales.

Wide Angle X-Ray Diffraction (WAXD). WAXD patterns were recorded in reflection geometry by a Philips X'Pert PRO diffractometer equipped with a graphite monochromator on the diffracted beam (CuK_α radiation). The angular range for the measurements in the reflection geometry was 5-40° 2θ. A least-square fit procedure was applied according to Hindeleh and Johnson[25] to reproduce WAXD profiles and to determine the degree of crystallinity.

Small Angle X-Ray Scattering (SAXS). The SAXS patterns of the samples were recorded by an MBraun system, utilizing CuK_α radiation from a Philips PW 1830 X-ray generator. The data were collected by a position sensitive detector, in the scattering angular range 0.1-5.0° 2θ and they were successively corrected for blank scattering.

A constant continuous background scattering was then subtracted[26] and the obtained intensity values $\tilde{I}(s)$ were smoothed in the tail region, with the aid of the $s \cdot \tilde{I}(s)$ vs. $1/s^2$ plot.[27]

Finally, the Vonk's desmearing procedure[28] was applied and the one-dimensional scattering function was obtained by the Lorentz correction $I_1(s) = 4\pi s^2 I(s)$, where $I_1(s)$ is the one-dimensional scattering function and $I(s)$ the desmeared intensity function, being $s=(2/\lambda)\sin\theta$.

SAXS Data Analysis. The evaluation of the SAXS patterns according to some theoretical distribution models[29,30] was carried out referring to the Hosemann model,[31] that assumes the presence of lamellar stacks having an infinite side dimension. This assumption takes into account a one-dimensional electron density change along the normal direction to the lamellae.

Hosemann[31] has shown that the observable intensity profile in the plane of the normal and incident ray can be splitted into two components:

$$I(s) = I^{I}(s) + I^{II}(s) \tag{1}$$

where:

$$I^{I}(s) = \frac{(\rho_Y - \rho_Z)^2}{4\pi^2 s^2 X} \times \frac{|1-F_Y|^2(1-|F_Z|^2) + |1-F_Z|^2(1-|F_Y|^2)}{(1-F_Y F_Z)^2} \tag{2}$$

$$I^{II}(s) = \frac{(\rho_Y - \rho_Z)^2}{2\pi^2 s^2 XN} \times Re\left\{\frac{F_Z(1-F_Y)^2(1-(F_Y F_Z)^N)}{(1-F_Y F_Z)^2}\right\} \tag{3}$$

In these equations, ρ_Y and ρ_Z are the electron densities of the crystalline and amorphous regions, respectively, N is the number of layers in the system and X the average long period, F_Y and F_Z represent the Fourier transforms of the distribution functions of the crystalline (Y) and of the amorphous (Z) regions e.g.:

$$F_Y = \int H(Y)\exp(-2\pi i s Y)dY \tag{4}$$

where $H(Y)$ is the normalized distribution for the crystalline thickness (the same definition provides the corresponding distribution for the amorphous region).

When N becomes large enough to be effectively infinite, the term I^{II} becomes negligible so that the observed intensity is given entirely by I^{I}. When N is reduced, I^{II} can no longer be neglected, with the effect of broadening the diffraction peak.[31]

A fitting procedure of the calculated one dimensional scattering functions with the experimental ones allows to optimise the values of the high and low density region thicknesses. Crystallinity (ϕ_{SAXS}) was evaluated as the ratio between the thickness of the high density regions over the long period $X=Y+Z$.

If a double population of lamellae is to be used, the intensity functions $I(s)$ will be calculated for each population such as to obtain the experimental pattern as a sum of the spectra of the two populations, each one corresponding to a different set of parameters.

Another commonly used approach for SAXS data analysis is that based on the correlation function.[32] The method described earlier was preferred because its results are solely based on SAXS. In the correlation function data treatment, in fact, WAXD crystallinity is employed for the estimation of the lamellar thickness, while our technique yielded lamellar parameters only on the basis of the SAXS profile. Moreover, the method used in this paper allows to obtain a larger number of morphological parameters, like the distribution of the thicknesses and of the crystallinity associated to the lamellar stacks, that can not be evaluated by the analysis of the correlation function. The reliability of the method described in this paragraph was also successfully checked by comparison with transmission electron microscopy measurements.[33,34]

Results

A DSC scan was performed on the samples. Figure 1 shows the obtained results. As may be seen, there is a striking difference between sample iPS10t and the others. In the thermogram of iPS10t a very wide exothermal peak appeared at about 150 °C, followed by an endothermic signal at 222 °C.

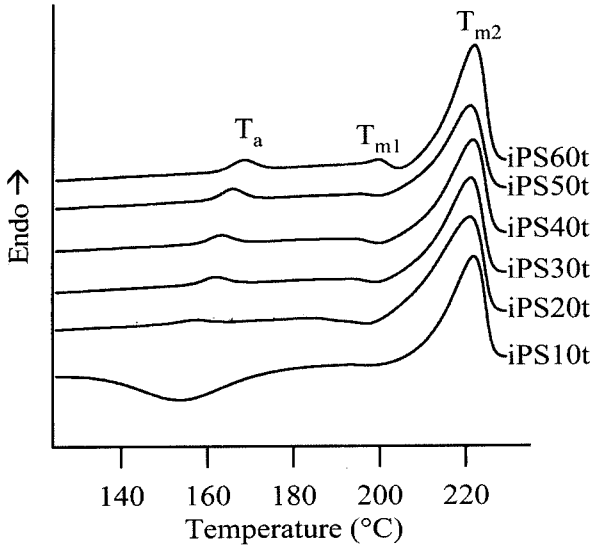

Figure 1. DSC traces of the samples crystallized for different times. The three temperatures T_a, T_{m1}, and T_{m2} are shown for sample iPS60t.

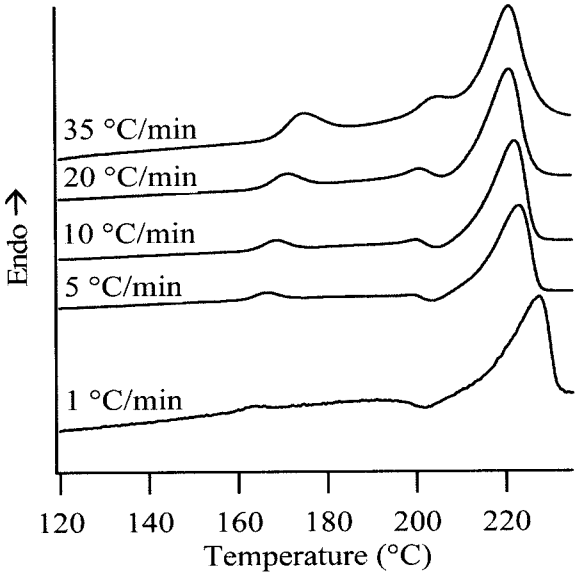

Figure 2. DSC traces of sample iPS60t recorded at different heating rates.

This behaviour is consistent with that of an amorphous iPS sample. So it can be concluded that 10 min were not sufficient for the sample to crystallize. All the other samples had, on the other hand, a similar DSC pattern, with three endotherms, at the temperatures designated T_a, T_{m1}, and T_{m2}, in order of increasing temperature. In sample iPS20t the peaks at T_a and T_{m1} were not well developed yet, while the signal corresponding to T_{m2} was clearly distinguishable.[21] Comparing samples crystallized for increasingly longer times (Figure 1), it can be noted that the endotherm at T_a shifted to higher temperatures, although remaining around the annealing temperature (160 °C), and its intensity increased. The endotherm at T_{m1} tended also to shift towards higher temperatures as the crystallization time increased. This peak was not always very clearly visible, principally because of an exothermal signal located between the two endotherms at T_{m1} and T_{m2}. This is due to a melting-recrystallization process taking place during the DSC scan.

Differently from the other peaks in the thermogram, the one at T_{m2} was always at 222 °C and appeared independent from the crystallization time. The entity of the melting-recrystallization phenomenon was studied by performing DSC experiments at varying heating rates. The results are displayed in Figure 2 for sample iPS60t. As the heating rate increased, the low temperature endotherms increased in peak temperature and size, while T_{m2} shifted towards lower values. This is compatible with melting-recrystallization.[6] A faster heating rate implies that the amount of crystalline regions that had time to recrystallize decreased, resulting in a smaller high temperature melting endotherm and a larger peak at T_{m1}. This effect can also be found in the increasing importance of the exothermal recrystallization peak as more time for reorganization is allowed, i.e. at low heating rates. This signal tends to cancel the one at T_{m1} out. Coalescence of the peaks at T_{m1} and T_{m2} begun for heating rates higher than 35 °C/min.

An analogous behaviour, either in the appearance of the DSC traces and in the dependence on heating rate was observed for the samples crystallized at different temperatures. The effect of increasing temperature corresponded to that of lengthening the duration of crystallization (Figure 3). As can be seen, increasing the crystallization temperature produced a shift in the position of the annealing peak, which

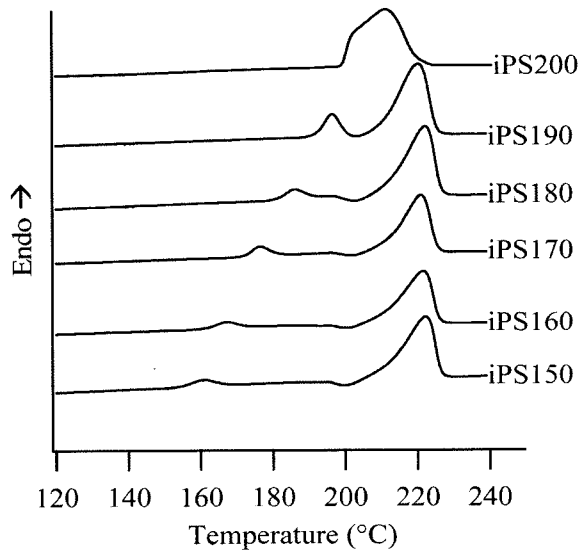

Figure 3. DSC traces of the samples crystallized at different temperatures.

was always about 10 °C beyond the crystallization temperature. For samples iPS190 and iPS200, T_a and T_{m1} were respectively equal and very similar, and so the multiple endotherms coalesced. In the thermogram of iPS200, it can be seen that the endotherm at T_{m2} is shifted to lower temperatures and merges with the other peaks at T_a and T_{m1}. In this case the crystallization temperature was very close to the melting temperature, so the resulting lamellae were thinner, with a consequent lowering of T_{m2}. This effect is also evident in sample iPS190, in which the crystallization temperature T_{m2} shifted to lower temperatures than the other specimens. At the same time, a slight increase of T_{m1} at high crystallization temperatures was expected, since at higher temperature crystallization proceeds more slowly, and daughter lamellae have a longer time to perfection themselves, attaining a higher melting temperature.

WAXD was used to study the semicrystalline framework of the considered samples. Figure 4 shows the WAXD patterns of samples iPS10t, iPS20t, and iPS60t. iPS10t is still practically amorphous, with a diffractogram analogous to that of iPSQ, while iPS20t and all the other samples had the WAXD pattern of a semicrystalline iPS. Employing a bimodal amorphous halo like that of iPS10t and iPSQ, the WAXD patterns of the samples were fitted and their degrees of crystallinity (ϕ_{WAXD}) obtained. Lorentzian functions were employed in the fitting procedure. iPS10t had a negligible ϕ_{WAXD}, while going from iPS20t to iPS60t a steady increase in ϕ_{WAXD} was observed from 35% in iPS20t to 47% for iPS60t. Between 10 and 20 min, the degree of crystallinity steeply increased to gradually level up when crystallization proceeded for longer times. When the effect of crystallization temperature was considered, no significant difference was observed among samples, with a constant ϕ_{WAXD} for all of them.

The lamellar morphology of the samples was investigated by SAXS. The SAXS patterns were fitted by a double population model, since no single population model allowed an accurate reproduction of the experimental profile. The obtained results are shown in Table I. The presence of two well defined populations can be seen in Figure 5. iPS10t did not produce a significant SAXS peak.

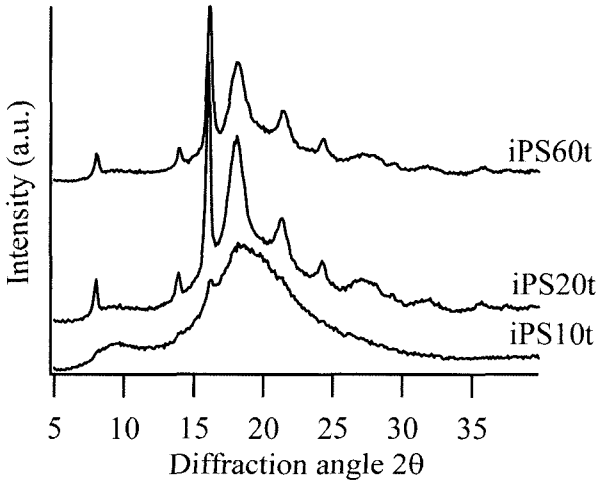

Figure 4. WAXD patterns of samples iPS10t, iPS20t, and iPS60t.

Table I. Crystalline (Y) and Amorphous (Z) Layers Average Thicknesses, Long Period (X), Thickness Distribution Values (σ_Y/Y, σ_Z/Z, and σ_X/X) Determined by SAXS. Subscripts 1 and 2 Denote the First and Second Lamellar Population, Respectively

	iPS20t	iPS30t	iPS40t	iPS50t	iPS60t
Y_1 (Å)	43	47	51	55	55
Z_1 (Å)	58	53	51	50	50
X_1 (Å)	101	100	102	105	105
σ_{Y1}/Y_1	0.3	0.3	0.2	0.1	0.2
σ_{Z1}/Z_1	0.3	0.3	0.2	0.1	0.2
σ_{X1}/X_1	0.2	0.2	0.2	0.1	0.1
Y_2 (Å)	27	28	30	36	37
Z_2 (Å)	36	32	30	32	34
X_2 (Å)	63	60	60	68	71
σ_{Y2}/Y_2	0.5	0.5	0.4	0.25	0.3
σ_{Z2}/Z_2	0.5	0.5	0.4	0.25	0.3
σ_{X2}/X_2	0.5	0.3	0.3	0.2	0.2

In the first population, the thickness of the crystalline layer (Y_1) increased with time, while that of the amorphous layer (Z_1) had an opposite trend. As the time of crystallization went from 20 to 60 min, the long period (X_1) slightly increased and the distribution of these parameters, i.e. X_1, Y_1, and Z_1, became narrower, signifying that allowing a longer time for crystallization produced more homogeneous and thicker lamellae.

For what concerns the second population, it formed since the first stages of crystallization, as it appeared after a 20 min

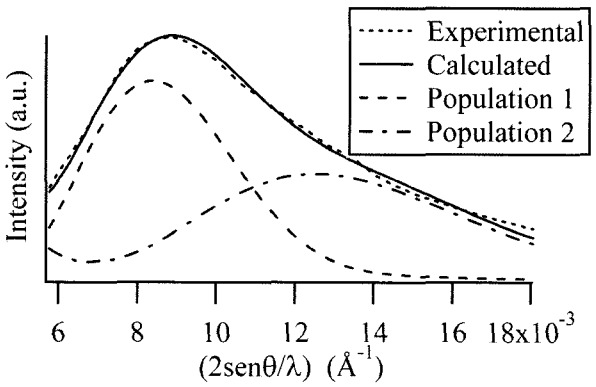

Figure 5. Fit of the SAXS pattern of sample iPS60t. The curves relative to each lamellar population are also shown.

annealing. The trends of the crystalline (Y_2) and amorphous (Z_2) layers for this population are similar to those of the first one, whereas the long period (X_2) increases more significantly. As expected in the case of a secondary crystallization process, lamellae pertaining to this population are much thinner than in the other one, and are consequently less thermically stable. The narrowing of the distribution of this population also is a sign that lamellar stacks become more perfect as time passes. When the effect of the crystallization temperature was taken into account, no significant variation in the morphology of the two lamellar populations was detected among the samples. Actually a slight variation, in the same trend as time-dependent samples, was observed, but overall the lamellar morphology in specimens crystallized at different temperatures was much more homogenous, given the fact that crystallization was allowed enough time to go to completion. This determined a levelling off of the morphological parameters of the stacks, except in the case of iPS190 and iPS200, where crystalline lamellae of the first population were found to be thinner than in the other samples. This confirmed DSC results in which T_{m2} was shifted at lower temperatures, and was due to the fact that a high crystallization temperature, too close to the melting temperature, did not favour the crystallization of the less regular portions of the polymer chains, resulting in thinner lamellae.

Discussion

The nature of the annealing peak has been often attributed to the melting of impurities[2] or of a second population of lamellae produced by secondary crystallization.[3,35] In order to explain the phenomenon originating this endothermal signal, temperature-dependent SAXS experiments were performed on one of the samples, iPS170. SAXS patterns were taken at temperatures corresponding to those indicated in the thermogram of Figure 6 and are shown in Figure 7, along with the fitting of experimental spectra. As can be seen, the two populations of lamellae initially present in the sample become more similar as temperature increases and finally coalesce into a single peak. As different theoretical models were necessary to fit experimental data (a double population up to 207 °C and a single population beyond that temperature) only qualitative considerations can be done. Nonetheless, it

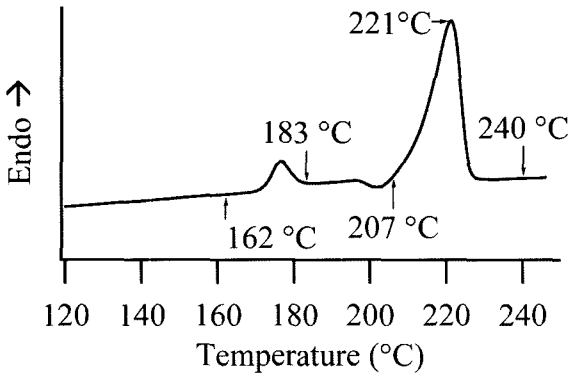

Figure 6. DSC trace of iPS170, showing the temperatures at which WAXD and SAXS spectra were acquired during temperature-dependent experiments.

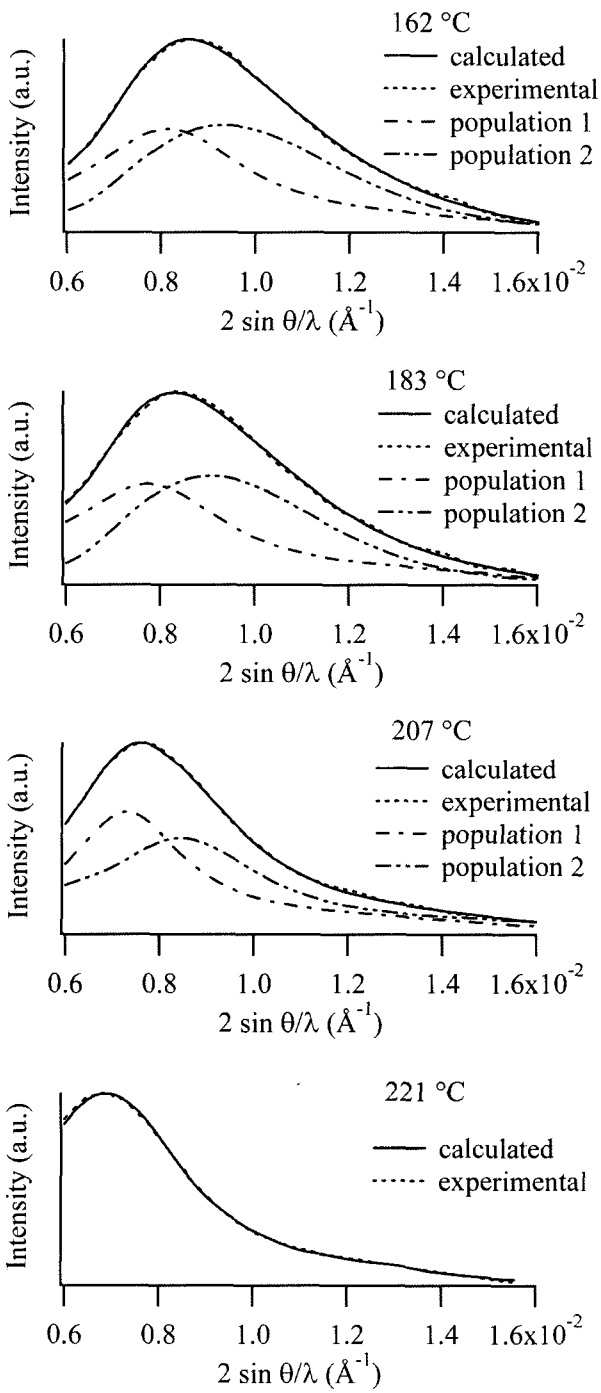

Figure 7. SAXS profiles of sample iPS170, acquired during the temperature-dependent experiment. The SAXS pattern at 240 °C was featureless and is not shown.

is remarkable that before and after the annealing peak the presence of a second lamellar population persists. Therefore, the possibility that the signal at T_a is originated by the melting of some crystalline population must be ruled out. Our results confirmed the second main hypothesis set forth to explain the nature of the annealing peak. According to a number of authors,[20-24] in fact, this signal is due to a relaxation of a pseudo-crystalline interphase towards a relaxed amorphous phase.[20,21,36] This peak was also associated to a mobilization of a rigid amorphous third phase.[23,37,38] A further proof that no crystal population is involved in the formation of the annealing peak and that this is due indeed to a relaxation phenomenon was sought with a temperature-controlled WAXD experiment. WAXD spectra were taken for sample iPS170 before and after T_a, at 162 and 183 °C, respectively. The two patterns were superimposable (Figure 8), signifying that no change whatsoever occurred in the semicrystalline framework in correspondence to the annealing peak.

Since two lamellar populations resulted from SAXS analysis, the attribution of the higher temperature melting peaks to regions of different thermal stability within the same lamella[20-23] could be ruled out in the case of our samples.

The two populations detected in the SAXS analysis are partly responsible for the appearance of the two melting peaks at higher temperature in the thermograms. These populations form since the earliest stages of crystallization. Daughter lamellae formed in the secondary crystallization process acquire progressively more thermal stability the longer they are allowed to grow, while dominant ones attain always the same degree of order, as they always melt at 222 °C. Along with these two coexisting lamellar morphologies, a melting-recrystallization phenomenon is present during the DSC heating scan. This was confirmed by the appearance of an exothermal peak between T_{m1} and T_{m2} and by the shift of the signals as a consequence of a varying heating rate. The concurrence of melting-crystallization and of a complex lamellar morphology as the cause of a multiple melting behaviour has already been reported.[21] As may be seen in Figure 7, the first melting peak should be attributed to the melting of the second lamellar population, characterized by thinner and less thermically stable lamellae. Passing from 183 to 207 °C, i.e. before and after the melting peak at T_{m1}, it can be noted that the intensity of the second population significantly decreases, without disappearing just because of the effect of recrystallization. Moreover, the overall SAXS peak considerably sharpens and the long period increases as a consequence of the disappearing of the second population (Figure 7). At T_{m2}, that in the case of iPS170 was at 223 °C, the recrystallization process brought about a thickening of the second population that merged with the first, leaving just one, with a large long period, that melts giving rise to the second main melting peak (Figure 7).

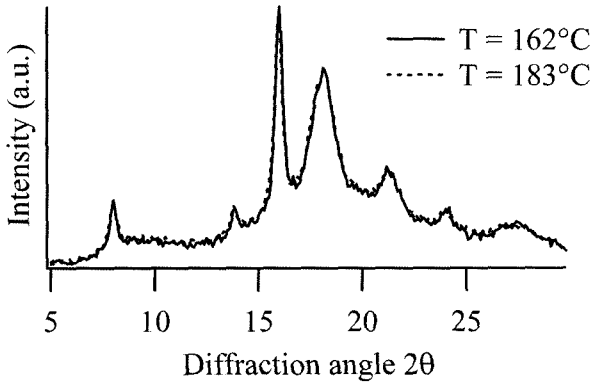

Figure 8. WAXD patterns of sample iPS170 taken at temperatures before and after the annealing peak.

It remains to be understood if the second population of subsidiary lamellae exists within the main lamellar stacks (lamellar insertion model)[13-15] or if it is a separate entity with respect to the main lamellar stacks (dual stack model).[12,16] This could be explained by the WAXD and SAXS analysis of the samples prepared with different crystallization times. Table II shows the integrated areas of the SAXS peaks due to the two populations of lamellae. The area of population 2 increases more than that of population 1. The area of the population 1 peak increased by 17%, while that of population 2 had a 28% increment. This means that the thickening and ordering of population 2 lamellae is more extensive than that of population 1, in which lamellae form already with a significant regularity, less affected by crystallization time. This is in good accord with a model that includes a primary crystallization in which lamellae are thick and attain quite rapidly a stable structure that does not vary with time, and a secondary crystallization that generates thinner and less stable lamellae that require a longer time to crystallize.

Comparing the volumetric crystallinities of the samples, differences can be noted between those obtained by WAXD and SAXS (Table III). This divergence can be explained considering the difference between the two techniques. WAXD allows the detection of all the crystalline forms in the sample, while SAXS is only sensitive to the regions organized in lamellar stacks. The lower crystallinity obtained by WAXD is thus due to amorphous domains that are external to lamellar stacks, not detected by SAXS. The trend of the difference

Table II. Integrated Area, in Arbitrary Units, of the SAXS Peaks Relative to the First and Second Lamellar Population

Sample	Area Population 1	Area Population 2
iPS20t	45	35
iPS30t	49	37
iPS40t	50	37
iPS50t	54	49
iPS60t	49	46

Table III. Volume Crystallinities Determined for the Different Samples by WAXD (ϕ_{WAXD}) and SAXS (ϕ_{SAXS}) and Difference between the Quantities Obtained by the Two Techniques

	iPS20t	iPS30t	iPS40t	iPS50t	iPS60t
ϕ_{WAXD} (%)	35	36	39	44	47
ϕ_{SAXS} (%)	43	47	50	52	52
ϕ_{SAXS} - ϕ_{WAXD} (%)	8	11	11	8	5

between ϕ_{WAXD} and ϕ_{SAXS} contributed to shed some light on the best model to use in order to describe the two lamellar populations. If a semicrystalline polymer is considered, in which extralamellar amorphous dominions exist, WAXD crystallinity will be given by the ratio of the crystalline material (organized in lamellar stacks) C_{stack} over the sum of C_{stack}, of the intralamellar amorphous A_{stack} and of the extralamellar amorphous dominions A_{extra}:

$$\phi_{WAXD} = \frac{C_{stack}}{C_{stack}+A_{stack}+A_{extra}} \tag{5}$$

SAXS crystallinity, on the other hand, will be dependent on the crystalline and amorphous polymer within the stacks and not on extralamellar material:

$$\phi_{SAXS} = \frac{C_{stack}}{C_{stack}+A_{stack}} \tag{6}$$

Supposing that as a consequence of the formation of new lamellae within the existing stack (lamellar insertion model)[13-15] (Figure 9(a)) the quantity of crystalline material increases by ΔC, ϕ_{WAXD} and ϕ_{SAXS} will be influenced in different ways:

$$\phi'_{WAXD} = \frac{C_{stack}+\Delta C}{(C_{stack}+\Delta C)+(A_{stack}-\Delta C)+A_{extra}} \tag{7}$$

$$\phi'_{SAXS} = \frac{C_{stack}+\Delta C}{(C_{stack}+\Delta C)+(A_{stack}-\Delta C)} \tag{8}$$

WAXD crystallinity will increase by a lesser extent because the quantity of crystalline material is "diluted" by the extralamellar amorphous:

$$\Delta\phi_{WAXD} = \phi'_{WAXD}-\phi_{WAXD} = \frac{\Delta C}{C_{stack}+A_{stack}+A_{extra}} \tag{9}$$

$$\Delta\phi_{SAXS} = \phi'_{SAXS}-\phi_{SAXS} = \frac{\Delta C}{C_{stack}+A_{stack}} \tag{10}$$

If the new lamellae are formed outside the existing lamellar stacks, as in the dual lamellar stacks model[12,16] (Figure 9(b)), the WAXD and SAXS crystallinities will be affected in a different way with respect to the preceding case:

$$\phi''_{WAXD} = \frac{C_{stack}+C_{stack2}}{C_{stack}+C_{stack2}+A_{stack}+A'_{extra}} \tag{11}$$

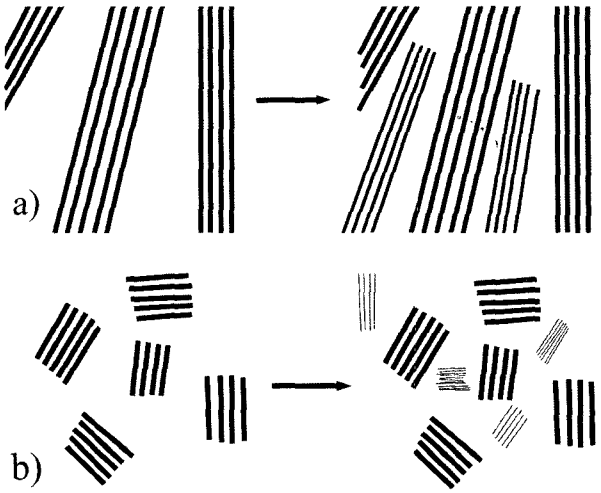

Figure 9. Schematic of the lamellar insertion model (a) and of the dual lamellar stack model (b). Black lines represent iPS lamellae.

$$\phi''_{SAXS} = \frac{C_{stack}+C_{stack2}}{C_{stack}+C_{stack2}+A_{stack}+A_{stack2}} \tag{12}$$

where C_{stack2} and A_{stack2} represent the crystalline and amorphous material, respectively, of the second lamellar population and $A'_{extra} = A_{extra} - C_{stack2}$.

In this case, the formation of new lamellae determines a decrease in the quantity of extralamellar amorphous material, and therefore a more rapid increase in WAXD crystallinity than that of SAXS crystallinity:

$$\Delta\phi''_{WAXD} = \phi''_{WAXD}-\phi_{WAXD} = \frac{C_{stack2}}{C_{stack}+A_{stack}+A_{extra}} \tag{13}$$

$$\Delta\phi''_{SAXS} = \phi''_{SAXS}-\phi_{SAXS} = \frac{C_{stack2}A_{stack}-C_{stack}A_{stack2}}{(C_{stack}+C_{stack2}+A_{stack}+A_{stack2})(C_{stack}+A_{stack})} \tag{14}$$

From the data in Table III, it can be seen that the difference in crystallinity tends to decrease as crystallization time passes. This means that WAXD crystallinity increases more rapidly than SAXS crystallinity and therefore that the second population grows according to the dual lamellar stack model and is located in the regions between pre-existing lamellar stacks. The crystallization of iPS can therefore be described as follows. The sample is initially amorphous, but it is not homogeneous and identical in every point of the bulk, there are in fact chains that, mainly because of their microstructure, can better order themselves and that are thus favoured in their crystallization process. From the nuclei, crystallization proceeds in two ways: more regular chains form thick dominant lamellar stacks, while the less regular molecules, by secondary crystallization, develop with time subsidiary stacks, much smaller and with a large distribution

of thicknesses. These tend to gradually occupy the amorphous zone, even though amorphous regions resist and are formed by the most irregular chains.

Conclusions

WAXD, SAXS, and DSC were employed to elucidate the structure and morphology of cold crystallized iPS and its multiple melting behaviour. The following model seems appropriate to describe iPS:

- this polymer crystallizes according to the dual lamellar stack model, with subsidiary lamellae forming by secondary crystallization in the regions between pre-existing lamellar stacks;
- the two lamellar populations give rise to the two higher temperature melting peaks: that at T_{m2} is due to the dominant stacks, that at T_{m1} to the subsidiary ones, although a melting-recrystallization phenomenon is present to some extent;
- the annealing peak is not due to the melting of crystalline material, but rather to the relaxation of a rigid amorphous phase.

Acknowledgements. V. C. gratefully acknowledges financial support by Basell Italia S.p.A., through a Federchimica grant, and by the University of Padova.

References

(1) J. Boon, G. Challa, and D. W. Van Krevelen, *J. Polym. Sci.*, **A2(6)**, 1791 (1968).
(2) Z. Pelzbauer and R. St. J. Manley, *J. Polym. Sci.*, **A2(8)**, 649 (1970).
(3) P. J. Lemstra, T. Kooistra, and G. Challa, *J. Polym. Sci.*, **A2(10)**, 823 (1972).
(4) J. Plans, W. J. MacKnight, and F. E. Karasz, *Macromolecules*, **17**, 810 (1984).
(5) D. J. Blundell, *Polymer*, **28**, 2248 (1987).
(6) Y. Lee, R. S. Porter, and J. S. Lin, *Macromolecules*, **22**, 1756 (1989).
(7) M. Al-Hussein and G. Strobl, *e-polymers*, 2002;38. http://www.e-polymers.org/papers/alhussein_110902.pdf [accessed 4 April 2006].
(8) M. Al-Hussein and G. Strobl, *J. Macromol. Sci. Phys.*, **B42**, 677 (2003).
(9) S. Z. D. Cheng, M. Y. Cao, and B. Wunderlich, *Macromolecules*, **19**, 1868 (1986).
(10) P. Cebe and S. D. Hong, *Polymer*, **27**, 1183 (1986).
(11) D. C. Bassett, R. H. Olley, and I. A. M. Al Raheil, *Polymer*, **29**, 1745 (1988).
(12) M. P. Lattimer, J. K. Hobbs, M. J. Hill, and P. J. Barham, *Polymer*, **33**, 3971 (1992).
(13) K. N. Krüger and H. G. Zachmann, *Macromolecules*, **26**, 5202 (1993).
(14) B. S. Hsiao, K. H. Gardner, and D. Q. Wu, *Polymer*, **34**, 3996 (1993).
(15) T. Y. Ko and E. M. Woo, *Polymer*, **37**, 1167 (1996).
(16) R. Verma, H. Marand, and B. Hsiao, *Macromolecules*, **29**, 7767 (1996).
(17) H. Marand and A. Prasad, *Macromolecules*, **25**, 1731 (1992).
(18) X. L. Ji, W. J. Zhang, and Z. W. Wu, *J. Polym. Sci., Polym. Phys. Ed.*, **35**, 431 (1997).
(19) N. Overbergh, H. Berghmans, and H. Reynaers, *J. Polym. Sci., Polym. Phys. Ed.*, **14**, 1177 (1976).
(20) T. Liu, S. Yan, M. Bonnet, I. Lieberwirth, K. D. Rogausch, and J. Petermann, *J. Mater. Sci.*, **35**, 5047 (2000).
(21) T. Liu and J. Petermann, *Polymer*, **42**, 6453 (2001).
(22) T. Liu, *Eur. Polym. J.*, **39**, 1311 (2003).
(23) H. Xu and P. Cebe, *Polymer*, **46**, 8734 (2005) and references therein.
(24) Y. Duan, J. Zhang, D. Shen, and S. Yan, *Macromolecules*, **36**, 4874 (2003).
(25) A. M. Hindeleh and D. J. Johnson, *J. Phys. D.: Appl. Phys.*, **4**, 259 (1971).
(26) C. G. Vonk and A. P. Pijpers, *J. Polym. Sci., Polym. Phys. Ed.*, **23**, 2517 (1985).
(27) C. G. Vonk, *J. Appl. Crystallogr.*, **6**, 81 (1973).
(28) C. G. Vonk, *J. Appl. Crystallogr.*, **4**, 340 (1971).
(29) D. J. Blundell, *Polymer*, **19**, 1258 (1978).
(30) C. Marega, A. Marigo, G. Cingano, R. Zannetti, and G. Paganetto, *Polymer*, **37**,5549 (1996).
(31) R. Hosemann and S. N. Bagchi, *Direct Analysis of Diffraction by Matter*, North Holland, Amsterdam, 1962.
(32) C. G. Vonk, in *Small angle X-ray scattering*, O. Glatter, and O. Kratky, Eds., Academic Press, London, 1982, p. 446.
(33) A. Marigo, C. Marega, R. Zannetti, and P. Sgarzi, *Eur. Polym. J.*, **34**, 597 (1998).
(34) V. Causin, C. Marega, A. Marigo, and G. Ferrara, *Polymer*, **46**, 9533 (2005).
(35) P. J. Lemstra, A. J. Schouten, and G. Challa, *J. Polym. Sci., Polym. Phys. Ed.*, **12**, 1565 (1974).
(36) M. Bonnet, K. D. Rogausch, and J. Petermann, *J. Colloid. Polym. Sci.*, **277**, 513 (1999).
(37) S. X. Lu and P. Cebe, *Macromolecules*, **30**, 6243 (1997).
(38) M. Al-Hussein and G. Strobl, *Macromolecules*, **35**, 1672 (2002).